http://www.ejchem.net

ISSN: 0973-4945; CODEN ECJHAO
E-Journal of Chemistry
2012, **9(3)**, 1373-1388

Alkali Activation of Oil Shale Ash Based Ceramics

A. HAMADI* and K. NABIH*

*Laboratoire de Chimie du Solide Appliquée, Faculté des Sciences, Département de Chimie
Avenue Ibn Batouta
B.P. 1014 Rabat, Morocco
hamadi_13@yahoo.fr

Recieved 10 June 2011; Accepted 13 August 2011

Abstract: Timahdit oil shale was subjected to firing transformation via ceramics processing followed by alkali activation to synthesis a materials combining the mechanical properties of ceramics and Zeolites. The mineralogical transformations during firing oil shale have been studied. The main crystalline phases found in oil shale ash (OSA) were wollastonite, gehlenite and augite. Modified oil shale ash (MOSA) was obtained with HNO_3 acid-leaching in the aim to diminish Ca content. Our experimental approach required a NaOH alkaline activating solution with different concentrations (0.5; 1; 2; 4; 6 and 8M). In our study, X-ray diffraction (XDR), Fourier transform infrared (FTIR) and SEM/EDS analysis were used to evaluate the effect of alkali activation on the structural arrangement of the starting materials (OSA and MOSA) in our study. The quantity and the type of the produced zeolites depended critically on the starting materials and on the NaOH concentration.

Keywords: oil shale, firing transformation, ceramics, alkali activation, Zeolites.

Introduction

Oil shale will be one of the most interesting energy and chemical sources in the world after the exhaustion of oil deposits. Morocco is one of the world leading countries in term of oil shale resources. These natural resources are very promising. They are estimated in Tarfaya deposit, located in the southwestern part of Morocco at 86 billion tons within a 2000 km^2 area and in Timahdet deposit, located about 250 km southeast of the capital Rabat, at 18 billion tons within a 196 km^2 area [1].

Mining and processing of the oil-shale will significantly disturb the environment, as a result of pollution by dust particles and ash derived from the oil shale [2, 3]. Valorisation of these valuable by product will reduce the environmental impact and will make oil shale development economically feasible for energy production in the future.

Oil shale ash (OSA) is used as raw material for cement and brick production [4,5,6]. Nevertheless the major amount is disposed as landfill. More efforts are required for developing new potential utilisations. Recently new processes are being investigated. The

similarity of mineralogical composition of oil shale ash with clay minerals has been reported [7]. Jingde et al [8] used a Chinese oil shale ash for the synthesis of glass-ceramics, which are usually produced from mineral clays. Hajjiji et al [9]studied the ceramics properties of Moroccan oil shale ash. Although , alkali activation of oil shale ash has been investigated for Zeolites production . Fernandes Machado et al [10]synthesized Na-A and –X Zeolites from Brazilian oil shale ash through two methods , studying the cristallinity of reaction products for each method. Shawabkeh et al [11] converted Jordanian oil shale ash to the Na-P1 zeolites and studied their potential applications for cation exchange capacity and adsorption propriety.

In our study we applied a ceramics processing to Timahdit oil shale followed by alkali activation of the resulting materials in the aim to combine the physical properties of ceramics and Zeolites materials. In order to optimize the experimental conditions oil shale ash heat treatment was carried out at 900° without any nucleating agent. Formation of augite simultaneously with gehlenite and wollastonite was characterized by X-ray diffraction (XRD), scanning electron microscopy (SEM) and Fourier transform infrared (FT-IR) spectroscopy. Alkali activation of the OSA via refluxing method was also investigated. The effect of starting material and the NaOH concentration on the Zeolites formation was discussed.

Materials and Methods

Timahdit oil shale used in our study was obtained from The ONHYM (Office National des Hydrocarbures et des Mines) [1]. Oil shale was grinded to small sizes (< 1 mm) and placed in porcelain crucibles. Samples were fired in a tubular laboratory furnace for 20 hours at 900°C under atmospheric conditions. The furnace power turned off leading a slow cooling down of the samples. Modified oil shale ash was obtained by an acid treatment of fired oil shale ash; the process was carried out as follow: 10 g was leached with 5M HNO_3 solution (40 ml) at ambient temperature with continuous stirring system for 24h. solid product were filtered-off, washed and dried at 100°C for 24h.The chemical composition of the oil shale ash (OSA) and the modified oil shale ash (MOSA) was determined by X-ray fluorescence (Philips, PW 2404, Magix Pro) (Table 1).

Table 1: Chemical composition of OSA and MOSA (%wt).

Compound	Oïl shale ash (OSA)	Modified oil shale ash (MOSA)
Na_2O	0.31	0.09
MgO	4.88	3.34
Al_2O_3	11.33	5.67
SiO_2	33.36	76.37
P_2O_5	1.31	0.07
SO_3	4.92	0.1O
K_2O	1.06	0.31
CaO	38.74	8.14
TiO_2	0.46	0.75
Fe_2O_3	3.31	4.81
MnO	0.03	0.02
Total	100.00	100,00

The synthesis method was based on the work of Henmi et al [12]. To understand the effect of NaOH concentration, a series of experiments were undertaken to determine phase chemistry of the products. Alkaline activation of oil shale ash was carried out as follow: 5g of OSA was mixed with 0.5,1, 2, 4, 6 and 8 M NaOH solutions (50 ml) in a Pyrex Becker, the mixture was stirred for 1 hour to create homogenous gel. Liquid /solid ration was fixed at 10. Refluxing process was carried out in Pyrex one-neck round-bottom flask in a heating mantle temperature was maintained at 100 °C. Heating period was fixed at 24 h for all experiments. Same process was followed for the Modified oil shale ash. Mineralogical composition of the starting materials and the reaction products was determined by X-ray by powder X-ray diffraction (PANalytical's X'Pert PRO X-ray diffractometer with Cu Kα radiation). Major and minor phases were performed with semi-quantitative method on the basis of the intensity (counts) of specific reflections, the density, and the mass absorption coefficient (Cu Kα) of the identified mineral phases [13, 14]. FTIR characterization of oil shale ashes and reaction products was conducted with a VERTEX 70 spectrometer equipped with digitec detector. The KBr pellet method was used to prepare the samples which were scanned in transmission mode with 4 cm^{-1} resolution at the range of 4000 to 400cm^{-1}. The morphology of oil shale ash and synthetic products was observed by JEOL JMS 5500 scanning electron microscope, equipped with SUTW-Sapphire detector for EDX analysis using a ZAF method for the quantification. The experimental conditions and the reaction products as well as the characterization tools are summarized in Table 2.

Table 2. Experimental conditions and characterization tools employed in the alkali activation of the oil shale ash (OSA) and the modified oil shale (MOSA).

		Experimental conditions				Characterization tools			
Starting material	Test symbol	NaOH concentration	L/S ratio (ml/g)	T(C°)	t(h)	XRD	FTIR	SEM/EDAX	Reaction products
Oil shale Ash (OSA) (5g)	ZB1	0.5	5	100	24	+	+		--
	ZB2	1	5	100	24	+	+	+	Tob
	ZB3	2	5	100	24	+	+		Tob
	ZB4	4	5	100	24	+	+	+	Tob, Can
	ZB5	6	5	100	24	+	+		Tob, Can
	ZB6	8	5	100	24	+	+	+	Tob, Can
Modified Oil shale Ash (MOSA) (5g)	Z'B1	0.5	5	100	24	+	+		--
	Z'B2	1	5	100	24	+	+		Ana
	Z'B3	2	5	100	24	+	+		Ana
	Z'B4	4	5	100	24	+	+	+	Ana
	Z'B5	6	5	100	24	+	+		Can
	Z'B6	8	5	100	24	+	+	+	Can

Tob: Tobermorite; Can: Cancrinite; Ana: Analcime.

Results and Discussion

Mineralogical characterization

The mineral phases of oil shale, as identified by XRD (not showed here), consists mainly of Calcite, Quartz, Dolomite and Clays .Minor phases include pyrite, hydroxyl-apatite, anhydrite and feldspars.

Oil shale ash (OSA) and Modified oil shale ash(MOSA)

During heat treatment, calcite, dolomite and clays have been decomposed respectively to CaO, MgO and Al_2O_3.Wollastonite [15]is the first abundant phase formed, resulting from the reaction of CaO with SiO_2 following the reactions of Peters and Iberg 1978[16](equation 1), while the reaction of CaO and SiO_2 with Al_2O_3 leads to the formation of gehlenite[17] (equation 2).Nevertheless gehlenite is considered as metastable phase in the presence of MgO and Fe_2O_3 which leads to the apparition of augite[18,19] (equation3).

$$CaCO_3\,(\text{Calcite}) + SiO_2 \rightarrow C0_2 + CaSiO_3\ \text{wollastonite}\ (1)$$

$$\text{illite}\ KAl_2(Si_3Al)O_{10}(0H)_2 + 6\ CaCO_3\ (\text{calcite}) \rightarrow 6C0_2 + 2H_2O + K_2O + 3SiO_2 +$$

$$3Ca2Al2Si2O7\ \ \text{gehlenite}\ \ (2)$$

$$Ca_2Al_2Si_2O_7 + CO_2 \rightarrow CaCO_3 + \ (Ca,Mg,Al,Fe)(Si,Al)O_3)_2\ \text{augite}\ (3)$$

The XRD spectrum of the oil shale ash shows also the presence of quartz [20] and anhydrite [21]. The existence of an amorphous phase is attested by the background noise (Fig. 1).

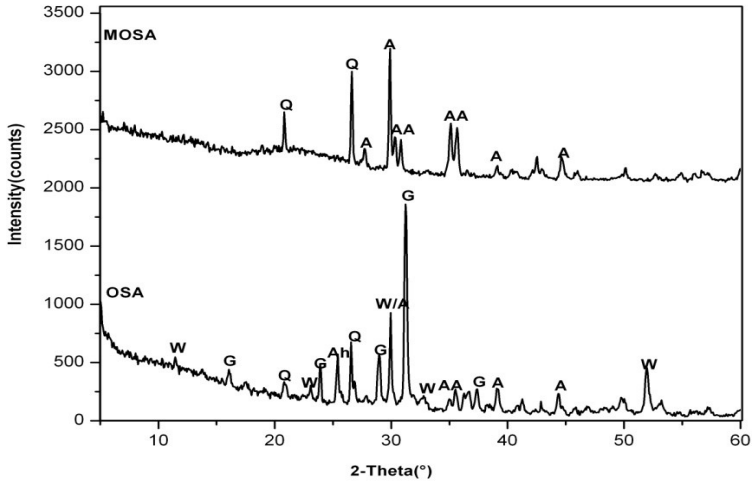

Figure 1. XRD patterns of oil shale ash (OSA) and modified oil shale ash (MOSA). Q: Quartz, W: Wollastonite, A: Augite, G: Gehlenite, Ah: Anhydrites.

After acid treatment only augite and quartz were present as shown by XRD (Fig.1). In fact these materials have a lower solubility in HNO_3 acid solution [22]. Based on semi-quantitative analysis, the mineralogical analysis of OSA and MOSA is shown in Table 3.

Table 3. Mineralogical analysis of Timahdet OSA and MOSA (% w/w).

Minerals	OSA	MOSA
Wollastonite	23.5	-
Gehlenite	13.9	-
Augite	20.3	34.3
Quartz	04.4	15.7
Anhydride	08.5	-
Amorphous	29.4	50.0

Alkali activated Oil shale ash (OSA)

The X-ray diffraction patterns of the activated oil shale ash with different NaOH concentration solutions are presented in fig. 2. When the OSA was activated with 0.5 M NaOH solution, the characteristic peaks of wollastonite, gehlenite and augite decreased this behavior continued with increasing NaOH concentration, nevertheless the dissolution of gehlenite was more important than augite and wollastonite. Dissolution of quartz started when the NaOH was set at 1 M, the intensity of the characteristic peak at 26.62 (2θ) decreased and tended to disappear in high NaOH solution. The 2θ position at 29.97 was supposed to decrease due to the alkaline attack, in contrast we observed this position growing more intense with increasing NaOH concentration, this can be explained by the formation of tobermorite [23] which have a basal reflection (220) at the same 2θ position as augite and wollastonite [24].It can also be observed the apparition of new peaks related to tobermorite. It should be noted that the persistence of augite and wollastonite is denoting the presence of tobermorite hence its presence was confirmed by SEM/EDX analysis. Cancrinite [25] is the main zeolitic phase formed and only when the concentration of NaOH solution is ≥ 2 M. The high percentage was realized for high NaOH concentration (9 %).

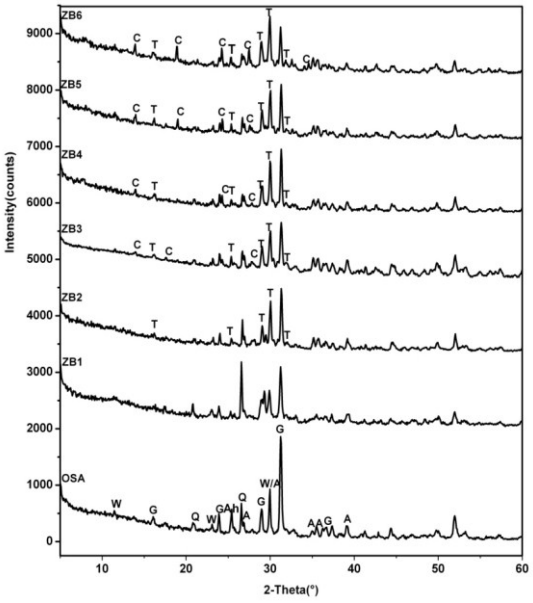

Figure 2. XRD patterns of alkali activated OSA.
Q: Quartz, W: Wollastonite, A: Augite, G: Gehlenite, Ah: Anhydrites T: Tobermorite, C: Cancrinite.

Alkali activated Modified oil shale ash (MOSA)

Fig.3 presents the X-ray diffraction patterns of the activated modified oil shale ash. We observed that the characteristic peak of quartz at 26.62 (2θ) increased with increasing NaOH concentration, while the characteristic peak of augite at 29.97 attaining the limit in 4 M NaOH solutions. The XRD pattern of the reaction product Z'B2 obtained in 1M NaOH solution shows the presence of analcime [26], this is the main zeolitic phase formed in this experimental conditions. The high cristallinity of analcime (25%) is observed in 4 M NaOH solution (Z'B4). When the NaOH concentration was > 4M, a minor cancrinite phase [27] was formed, the percentage of this Zeolites does not exceed 12%. This can suggests that the excess of NaOH concentration (>4M) plays a disadvantageous role on the Zeolites formation [22].

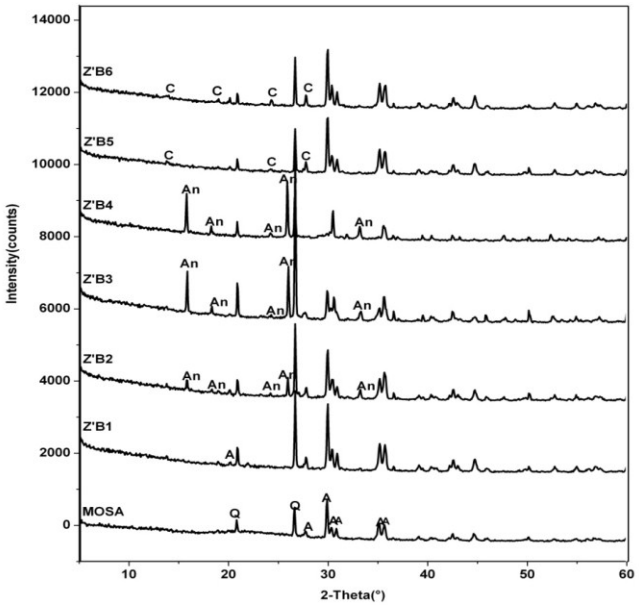

Figure 3. XRD patterns of alkali activated MOSA.
Q: Quartz, A: Augite, An: Analcime, C: Cancrinite.

Table 4. Identified minerals in Timahdet OSA and MOSA and in the reactions product.

Phase	Chemical formula	ICDD Card No	Reference
Wollastonite	$CaSIO_3$	84-0654	Ohashi Y. [15]
Gehlenite	$Ca_2Al_2SiO_7$	73-2041	Raaz F. [17]
Augite	$Al_{1,38}Ca_{0,74}Fe_{0,16}Mg_{0,01}O_6Si_{1,5}$	89-5691	Okui M. [18]
Quartz	SiO_2	46-1045	Kern A. [20]
Anhydride	$CaSO_4$	72-0503	Cheng G.C.H. [21]
Tobermorite	Ca_5 (O H)$_2$ $Si_2O_{16}.4(H_20)$	19-1364	Takahashi A. [23]
Cancrinite*	$Na_{7.86}(Al_6Si_6O_{24})(C0_3)(H_20)_{3.3}$	89-8047	Smolin Y. I.[25]
Analcime	$Na_{0,93}(AlSi_2\ O_6(H_2O)$	89-6324	Yokomori Y.[26]
Cancrinite**	$Na_8(AlSiO_4)_6(CO_3)(H_2O)_2$	72-2076	Hackbarth K. [27]

*: Cancrinite found in reaction products using OSA as starting material.

**: Cancrinite found in reaction products using MOSA as starting material.

The chemical form of each of the new minerals fond in Timahdet OSA and MOSA and the Zeolites found in reactions products is shown in Table 4, along with database powder diffraction file (PDF-2) from international center for diffraction data (ICDD) codes for XRD identification.

Fourier transformer infrared spectroscopy:

Oil shale ash (OSA)

The FT-IR spectrum in the region of 1200-400 cm^{-1} of the oil shale ash is illustrated in Fig. 4. The most intense bands are ranged between 1200 and 850 cm^{-1}, the next between 400–550 cm^{-1}, while the least intensive lies between 550–850 cm^{-1}.The bands in the 850-1200 cm^{-1} are attributed to the asymmetric stretching (O–Si–O) and (Si–O–Si) vibrations[28]. Referring to the work of Sterns[29], the bands with high intensities in this range can be attributed to Si-O(Si) bridge bonds rather than Si–O terminal bonds. Consequently, the two intense bands at 1020 and 971 cm^{-1} can be assigned to Si–O–Si bridge bonds. The signals at 937, 908 and 860 cm^{-1} are attributed to Si–O terminal bonds. According to literature, all of these bands can indicate the presence of wollastonite, gehlenite, and augite minerals in oil shale ash [29,30,31,32]. In the range of 850-550 cm^{-1} , three bands in oil shale ash spectrum due to the deformations of the Si–O–Si linkages, are detected at 567 cm^{-1}, 645and 677 cm^{-1} they are attributed to the wollastonite[31.32]. Besides them others signals were observed at 604, 712 and 825 cm^{-1} they were attributed to $SO_3^{2-}$and Carbonates. The last range between 550-400 cm^{-1} was less studied. In fact several bands with different vibration mode can overlap in this range. An assignment was mad according to literature. The bands located at 515 and 478 cm^{-1} can be attributed to bending $O_{(terminal)}$ –Mg–$O_{(terminal)}$ bonds vibration, while the band located at 422 and 437 cm^{-1} can be attributed to the stretching Al–O vibrations of the AlO_6 tetrahedra[30].

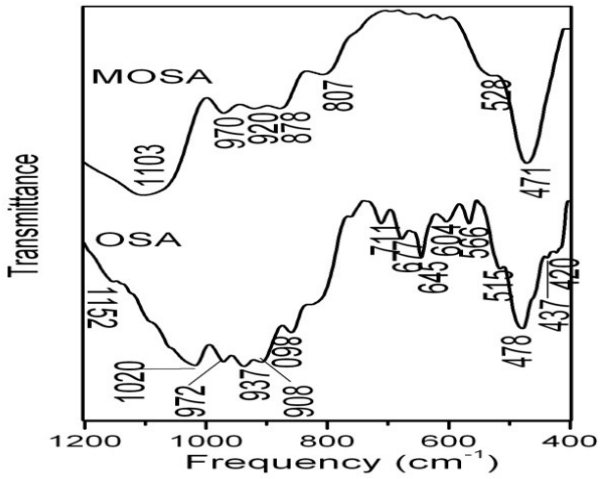

Figure 4. FTIR spectra of the firing oil shale (OSA) and the modified oil shale ash (MOSA).

Modified oil shale ash (MOSA)

The second FT-IR spectrum in Fig.4 represents the modified oil shale ash (MOSA) sample, in the region of 1200-400 cm^{-1}. The spectrum shows that the sample consist mainly of bands related to augite mineral (see Table 5).
The band appearing around at 1100 cm^{-1}, according to Hamilton [36] this broad band is commonly found in the spectra of augite with low (< 15%) Ca content, other characteristic band is centered at 972 cm^{-1} which can be attributed to stretching Si-O-Si bridge vibration, where as the bands located at 920 and 877 cm^{-1} corresponds to Si-O(Si) terminal vibration. Three bands with low intensities are located at 609, 638 and 665 cm^{-1} , they're attributed to the deformation of the Si–O–Si linkages. We notice that the band 638 cm^{-1} confirms the existence of crystalline structure of augite (Griffiths, 1987) [37]. The bands located at 528 and 471cm^{-1} can be attributed to the bending vibration of Si–O–Al linkages (lin and hwang, 1996) [38].

Table 5. The bands in FTIR spectrum of Augite compared to corresponding literature data.

Augite			
This work	Goel [26]	Makreski[27]	Nicodom [28]
1103 vs*	1072 vs	1075 vs	1070 vs
970 m	975 vs	974 s	965 vs
920 m	----	919 w	920 w
877 m	875 s	872 vs	865 s
665 w	674 w	673 w	675 w
638 w	638 m	634 m	635 m
528 m	520 m	521 m	510 m
471 vs	478 vs	469 vs	465 vs

*: s : strong, w : weak, m :medium, v : very.

Alkali activated Oil shale ash (OSA)

As showed in x-ray diffraction analysis, activated fired oil shale contains unreacted crystalline phases and Na aluminosilicates gel as principal product and zeolites as minority reaction products. Due to their similar constitution (SiO_4 and AlO_4 tetrahedra), the vibrations of the bands related to the different phases of the reaction products may certainly overlap, this situation can render the interpretation of their FTIR spectra more difficult [39].
The FT-IR spectra of activated oil shale ash are given in Fig.5. The bands at 1020 and 972 cm^{-1} which corresponds to Si–O–Si bridge vibrations, shifted slightly to lower frequencies with increasing NaOH concentration, suggesting a small structural changes of the Ca silicates materials present in oil shale ash and occurring the to the material a mechanical strength and alkali resistance properties . The bands at 860, 908 and 937 cm^{-1} which correspond to $Si–O^-$ terminal vibrations, show a decreasing behaviors in their intensities as NaOH concentration increase, still the band around 937 cm^{-1} tends to disappear Indicating

the polymerization of a new sodium aluminosilicates material. In the range of 500-800 cm^{-1}, new bands appeared in spectra of activated oil shale ash which is treated with NaOH concentration superior to 4M. The bands at 763 and 681 cm^{-1} are attributed to symmetric Al–O–Si vibration related to Zeolites materials, while the band at 623 cm^{-1} is attributed to the 6-memebered double-ring vibration of cancrinite [40,41].We should notice that the bands detected in this range are very weak. The band at 460 cm^{-1} which is attributed to the internal linkage of the TO_4 (T=SI, Al) tetrahedra related to zeolites materials can give us an information about the degree of crystallization of these materials [42].

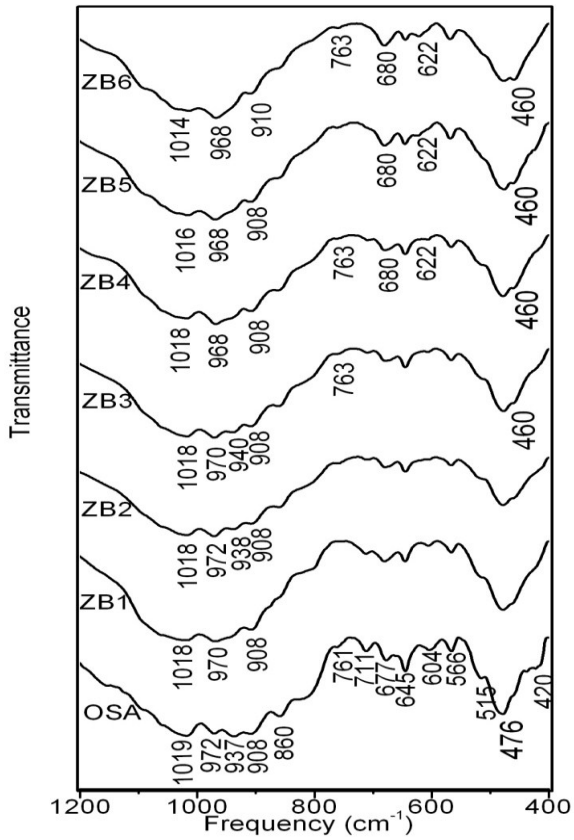

Figure 5. FTIR of the activated OSA.

Alkali activated Modified oil shale ash (MOSA)

The spectra of activated modified oil shale ash show interesting changes (Fig.6). As can be seen in the spectrum of the starting activation (0,5 M NaOH), the band at 1103 cm^{-1} observed in MOSA disappeared and a new band was formed at 1062 cm^{-1} associated to bridging stretching Si-O-Si_b (b:bridge) vibrations of the polymerized sodium aluminosilicates (Na-Al-Si-H). with increasing NaOH solution concentration, this band followed a pendular movement, moving first to lower and later moved back to higher frequencies , this behavior is related to Al/Si ratio of the reaction product, as reported early by Criado [43]. The second bridging stretching Si-O-Si_b vibrations at 970 cm^{-1} shifted slightly to higher frequencies than moved back to lower frequencies . The $Si–O^-$ terminal bonds observed initially in MOSA spectrum at 920 and 877 cm^{-1} decreased first in their

intensities with increasing NaOH concentration and later grow more intense. At relative Al rich gel, polymerized Na aluminosilicates grows with increasing of the number of bridge bonds (growing more intense) and decreasing of the number of terminal bonds. Nevertheless, increasing NaOH concentration leads to the formation of rich Silica gel .The band at 1032 cm^{-1} observed in MOSA treated with 4 M solution moved back to high frequencies and grows more intense. The $Si–O^-$ terminal bonds (920-875 cm^{-1}) shows an increasing behavior in their intensities. In connection with that, it may be considered that the excess of NaOH concentration decrease polymerization process of reaction products [22]. The new bands appeared in the range of 500-800 cm^{-1} in the spectra of activated MOSA with Al rich gel precursor at 667 and 765 cm^{-1} are attributed to the 4-memebered single-ring vibration of analcime, another bands are observed at 645 and 610 cm^{-1} which are due also to the same vibration referring to the literature [42,44,45].The bands defined at 800, 779 and 694 cm^{-1} are attributed to symmetric Si–O stretching vibrations in quartz .The band at 460 cm^{-1} is attributed to the internal linkage of the TO_4 (T=SI, Al) tetrahedra related to zeolites materials.

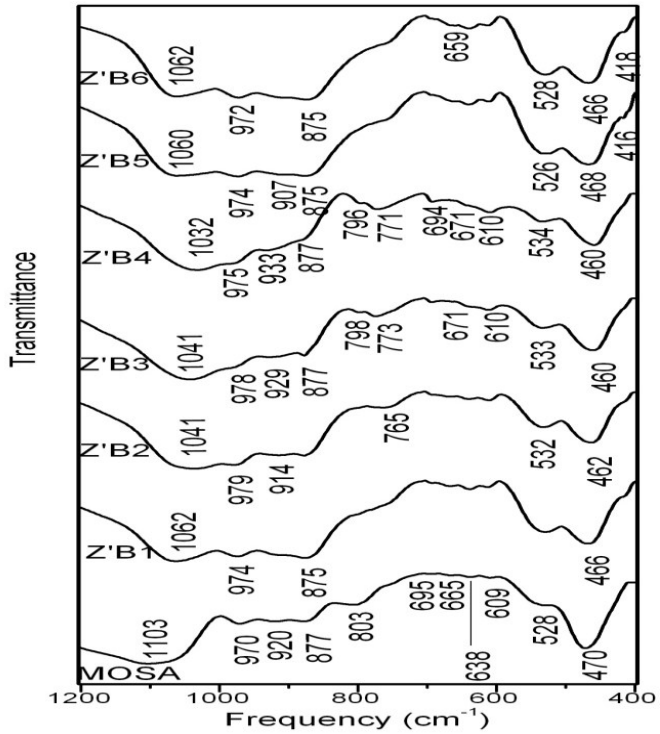

Figure 6. FTIR of the activated MOSA.

SEM-EDX testing

Oil shale ash (OSA)

The Major fired oil shale particles tends to be aggregated into a great deal of larger particles, which have a varied composition, with calcium and silicon as the dominant cations, and minor amounts of aluminum, magnesium, sulphur and iron. Scannining electron microscope of Fig. 7 shows the surface morphology of various observed structures. The most abundant of these structures has an elongated form [46]. On the other hand, quartz is present and can be seen clearly with Carbon deposed on its surface (fig. 8).

Scanning electron microscope of the OSA sample shows well crystallized acicular-type crystals (structure 1).This typical of the wollastonite type crystal formed at heat treatment temperature of 900° crystals which is the dominant phase [47]. Gehlenite occur as tetragonal-type structure (structure 2). On other hand, a brighten whisker (nanowires) type which was detected in different regions of the OSA sample is attributed to augite a glass-ceramic material (structure3).].Finally a clear pseudo-cubic structure is detected on the middle which can be attributed to Anhydrite mineral (structure 4).
The EDX patterns in fig.7 indicate that the most phases in the sample contain C, O, Mg, Al, Si and Ca. However it's clearly seen that nature of peak intensities corresponding to each element can help us to identify most structures, the compounds containing Si, O, Al and Ca with strong peak intensity may be identified as augite and gehlenite (structure 2 and 3).S was the predominant element in the structure 4, which confirmed the identification of this phase as anhydrite.

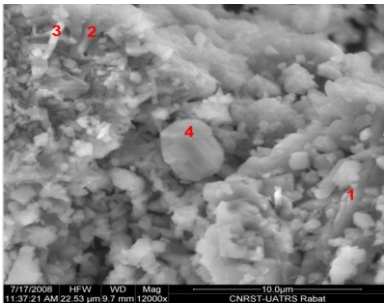

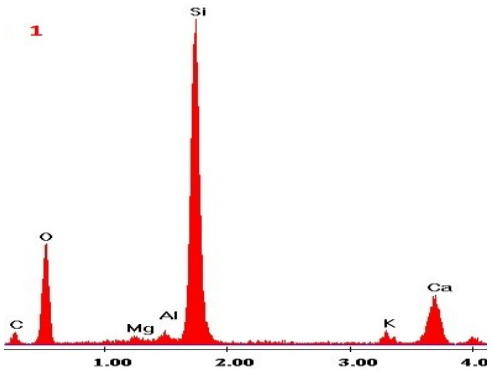

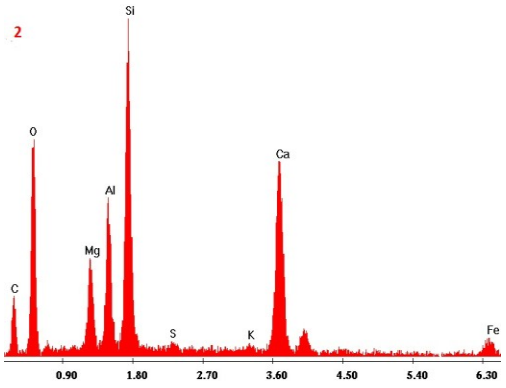

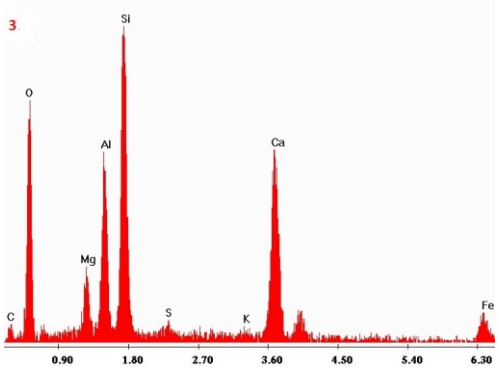

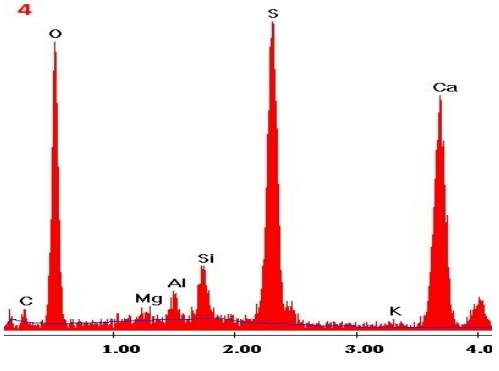

Figure 7. SEM and EDX images of OSA sample.
1: Wollastonite, 2: Gehlenite, 3: Augite and 4: Anhydrite.

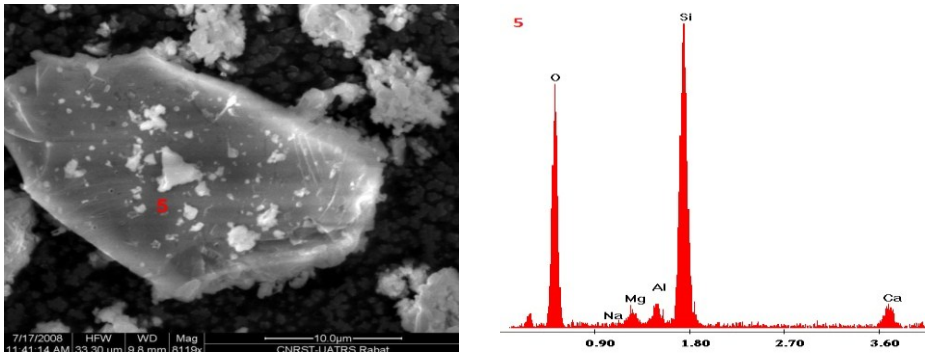

Figure 8. SEM image and EDX analysis of Quartz detected in OSA.

Modified oil shale ash (MOSA)

After acid treatment, only two phases were detected augite and quartz; as can be seen in Fig.9 the morphology of these phases is different from the first sample, we can observe more brighten aggregates related to amorphous phases. The EDX analysis of the modified oil shale ash shows a closer chemical composition but not the same peaks intensities.

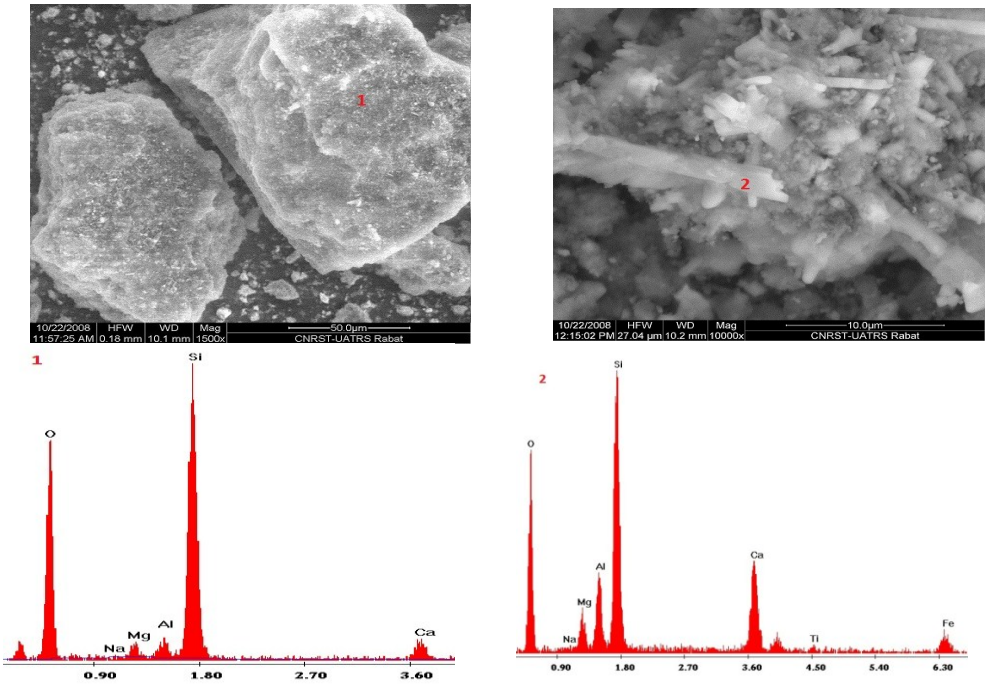

Figure 9. SEM and EDX of MOSA sample.

Alkali activated Oil shale ash (OSA)

SEM observation of the samples produced under alkali activation of OSA revealed two different morphologies. In the reaction products ZB2 and ZB4 prepared respectively with 1 and 4M NaOH concentration, a larger lath like structures were observed (Figs. 10-11(1)) , similar to those of the Al-substituted tobermorite [48] . Figures 10-11 (2) show the EDS spectrum of the lathlike structures. O, Ca and Si were detected as the predominant elements; it can be seen also the presence of the peaks related to Al, Mg and Na this confirms the incorporation of these elements in the lathlike structures of tobermorite.

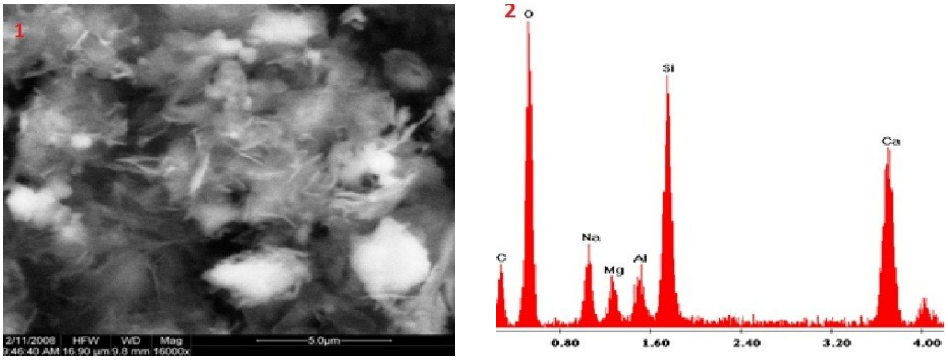

Figure 10. SEM (1) and EDX (2) of reaction product ZB2 (synthesized with 1M NaOH).

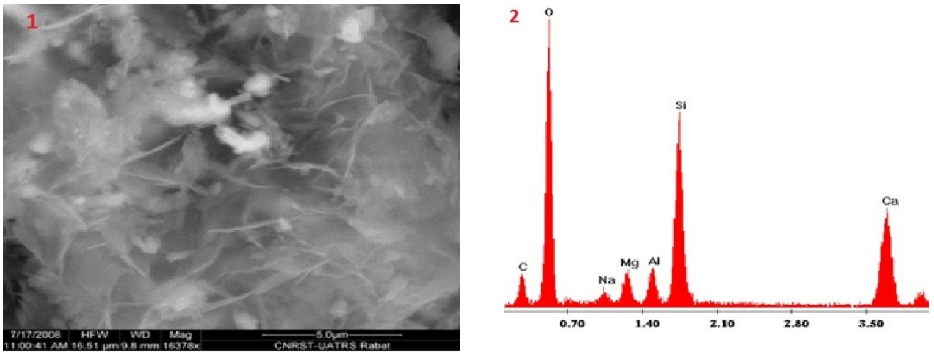

Figure 11. SEM (1) and EDX (2) of reaction product ZB4 (synthesized with 4M NaOH).

The second morphology observed in reaction products ZB6 consist of highly-crystalline cancrinite (Fig 12.1). The EDX analysis showed the presence of Carbonates and sulphates anions probably incorporated in cancrinite cage. Many previous works showed the role of those anions of the formation of high crystalline form of cancrinite [49].

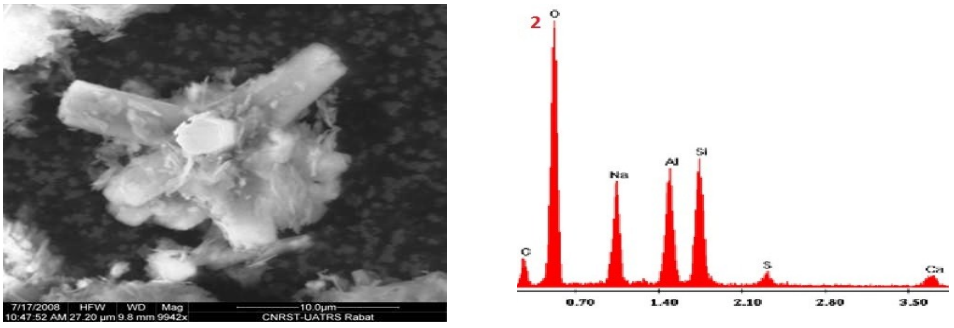

Figure 12. SEM (1) and EDX analysis (2) of the reaction product ZB6 (synthesized with 8 M NaOH).

Alkali activated Modified oil shale ash(MOSA)

SEM of Z'B4 sample a reaction products resulting from alkali activation of MOSA is shown in Fig13.1.A very small particles of analcime were detected in pseudo cubic form [50]. Nevertheless the Peaks position in XRD spectra matched closely with XRD PDF#89-6324 which the crystal system is trigonal. The EDX analysis reveals the presence of the Calcium probably in lime form (Fig. 13 .2).

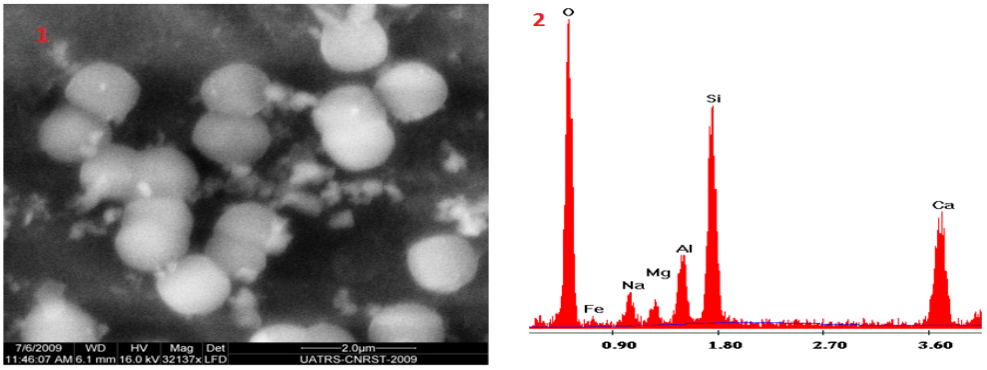

Figure 13. SEM (1) and EDX analysis (2) of the reaction product Z'B4 (synthesized with 4 M NaOH).

SEM of the Z'B6 sample MOSA is much more difficult to describe as the Fig 14 shows. It was almost impossible to detect the zeolitic material confirmed by x ray diffraction .This can be due probably to the presence of high percentage of amorphous phases in reaction products (>52%) [22].

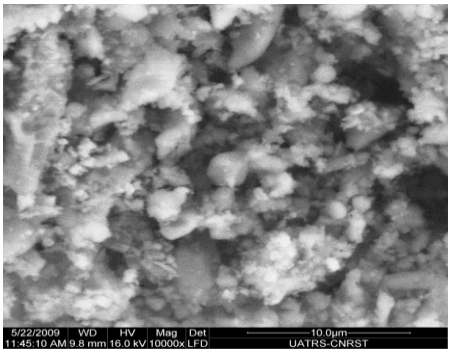

Figure 14. SEM of the reaction product Z'B6 (synthesized with 8 M NaOH).

Conclusion

The results presented here prove that the Oil shale ash and (OSA) contain significant proportions of wollastonite, gehlenite and augite. The new phases were formed as a consequence of Ceramics processing applied to Timahdet oil shale. Therefore, under acid treatment, only augite remains unchanged while gehlenite and wollastonite were completely dissolved.

Alkali activation treatment with NaOH solution of two different starting materials: oil shale ash (OSA) and modified oil shale ash (MOSA) has been studied. The experimental results provide many conclusions concerning the conditions of alkali activation of OSA and MOSA.

- DRX and FTIR analysis of alkali activated OSA suggest that gehlenite is the least resistant material compared with wollastonite and augite.
- Under alkaline conditions, gehlenite dissolved to release Ca, Al and Si.
- The presence of lathlike structure observed in reaction products synthesized with OSA and 1M NaOH solution is attributed to tobermorite. In addition the resulting tobermorite accommodates Al as shown by the EDS analysis.
- Dissolution of quartz increased with increasing NaOH concentration. Whereas Si content affect the crystallization of the reaction products.
- Cancrinite is developed as consequence of alkali activation of OSA (9 % for high NaOH concentration).
- Modified oil shale ash displays high reactivity in alkaline conditions. Pure phase of analcime was found in the reaction products. The optimum conditions were realized for 4M NaOH. However, when the NaOH concentration was set superior to 4M, a few amount of cancrinite (12%) was found suggesting that the excess of NaOH seems to cause deploymerization of aluminosilicates disfavoring the zeolites formation.
- Zeolites formation is critically affected by the NaOH concentration and Si/Al ratio.

Acknowledgements

Analytical instrument facilities were provided by the UATRS-CNRST (Unité d'Appui à la Recherche Scientifique-Centre National de la Recherche Scientifique et Technique), Rabat, Morocco. We are indebted to Mr. Zouihri Hafid for help with collecting X-ray powder diffraction, Mr. Dakhsi Khalid for assistance with SEM/ EDS collection and observations and Mr. Annour Khalid for FTIR analysis.

References

1. Office nationale des hydrocarbures et des mines (ONYHM). http://www.onhym.com/.
2. Jaber J O and Probert S D, App Energy, 1999, 62, 169-209.
3. Toomik A and Liblik V, Land Urb Plan., 1998, 41 285-292.
4. HE Y G, oil shale. 2004, 21(3), 259-264.
5. Smadi M M and Hadda R H, Cem Concr Comp., 2003, 25, 43-50.
6. Nabih K, Caractérisation et traitements thermiques des schistes bitumeux des sous couches R de Tarfaya sous différentes atmosphères (N2, He, air et vapeur d'eau), Utilisation du Ciment dans la production du ciment. D Etat thesis 1997 at university of Mohamed V (Rabat-Morocco).
7. Yoffe O, Nathan Y, Wolfarth A , Cohen S and Shoval S, Fuel, 2002, 81, 1101-17.
8. Jingde Luan, Aimin Li, Tong Su, Xiaobo Cui and Haza J, Mat.,2010, 143, 427-432.
9. Hajjaji M and Khalfaoui A, Cons Build Mater., 2009, 23, 959-966.
10. Fernandes Machado N R C and Malachini Miotto D M, Fuel, 2005, 84, 2289-2294.
11. Shawabkeh R , Al-Harahsheh A, Hami M and Khlaifat A, Fuel, 2004, 83,981-985.
12. Henmi T, Soil Sci Plant Nutr., 1987, 33, 519–523.
13. Beylrs P, Amer Miner., 1976, 61, 334-336.
14. Grzeta B and Popovic S, J Appl Cryst., 1985, 18, 80-84.
15. Ohashi Y and Finger L W, Amer Miner., 1978, 63, 274-288.
16. PETERS T and IBERGA R, Amer Ceram Soc Bull., 1978, 57, 503-509.

17. Korczak P and Raaz F, OEAW Math Naturwissenschaftliche Klasse., 1967, 104, 383-387.
18. Bowen N L, The evolution of igneous rocks; Princeton University press: NJ,1928, 321-322.
19. M. Okui , Haruo S and Fumiyuki M, Phys Chem Miner.,1998, 25, 318-322.
20. Kern A and Eysel W, Mineralogisch-Petrograph Inst Univ Heidelberg., Germany, ICDD Grant-in-Aid, 1993.
21. Swanson H E, Fuyar R K and Ugrinnic G M, Nat Bur Stand U.5. Circ., 1955, 539, 4-67.
22. Khale D and Chaudhary R, J Mater Sci., 2007, 42, 729–746.
23. The International Centre for Diffraction Data File No. 19-1364.
24. Shaw S, Clark S M and Henderson C M B, Chem Geo., 2000, 167, 129-140.
25. HACKBARTH K , GESING T M, FECHTELKORD M, STIEF F and BUHL J C, Micropor. mesopor. mater., 1999, 30, 347-358.
26. YOKOMORI Y and IDAKA I, Micropor Mesopor Mater.,1998, 21, 365-370.
27. Smolin Y I, Shepelev Y F, Butikova I K and Kobyakov I B, Soviet Phys Crys.,1981,26, 33–35.
28. Rutstein M S and White W B, Am Mineral., 1971, 56,877–887.
29. Sterns R G J. The common chain ribbon and ring silicates, in: V.C. Farmer (ED). Infrared spectra of Minerals. Mineralogical society London, UK, 1974.
30. Kimata M, N Jb Miner Abh., 1980, 139, 43–58.
31. Dowty E, Phys Chem Mineral, 1987, 14,122–138.
32. Omori K, Am Mineral., 197, 56, 1607–1616.
33. Goel A , Tulyaganov D U, Kansal I, Shaaban E R and Ferreira J M F, Inter J Mater Eng Innov., 2009, 1, 40-60.
34. Makreski P, Jovanovski G, Gajović A, Biljan T, Angelovsk D and Jaćimović R, J Mol Struc., 2006, 788, 102-114.
35. Nicodm. Inorganic library of FTIR spectra-Minerals, 1998.
36. Hamilton V E, J G R., 2000, 105, 9701-9716.
37. Griffiths P R, Clark R J H and Hester Eds R E, Recent Commercial Instrumental Developments in Fourier Transform Infrared Spectrometry; in Advances in Infrared and Raman Spectroscopy; Heyden Publishing Co: London,1983, vol.10, Chapter 5, 277-306.
38. Lin S-L and Hwang C-S, J Non-cryst solide., 1996, 202, 61-67.
39. Fernandez-Jimenez A, Palomo A, Micropor Mesopor Mater., 2005, 86, 207-214.
40. Barnes M C , ddai-Mensah A J and Gerson A R, Micropor Mesopor Mater.,1999, 31,287-302.
41. Zhao H, Deng Y, Harsh J B, Flury M and Boyle J S, Clays Miner., 2004, 52, 1-13.
42. Mozgawa W, Sitarz M and Rokita M, J Mol Struc., 1999, 511, 251-257.
43. Criado M, Fernandez-Jimenez A and Palomo Q, Micropor Misopor Mater.,2007, 106, 180-191.
44. Rios C A, Williams C D and Castellanos O M, Bistua, 2004, 4, 60-71.
45. Barbrieri E, corraadi A and Lanceloti I, Eur J Ceram Soc., 2000, 20, 1637-1643.
46. Cultrone G, Rodriguez-Navarro C, Sebastian E, cazalla O and De la torre M J, Eur J Mater., 2005, 13, 621-634.
47. Bernardo E, Bonomo E and Dattoli A, Ceram Inter., 2010, 36, 1675–1680.
48. Mostafaa N Y, Kisharb E A, Abo-El-Eneinc S A, J Allo Comp., 2009,473, 538-542.
49. Deng Y, Flury M, Harsh J B, Felmy A R and Qafoku O, App Geochem., 2006, 21, 2049-2063.
50. Sandoval M V, Henao, J A, Rios C A and Williams, D.C, Fuel, 2009, 88, 272-281.